Additive Manufacturing 18 (2017) 74–83

Contents lists available at ScienceDirect

Additive Manufacturing

journal homepage: www.elsevier.com/locate/addma

Full Length Article

# Digital light processing 3D printing of conductive complex structures

Quanyi Mu[a,b,1], Lei Wang[a,1], Conner K. Dunn[b], Xiao Kuang[b], Feng Duan[c], Zhong Zhang[c], H. Jerry Qi[b,*], Tiejun Wang[a,*]

[a] State Key Lab for Strength and Vibration of Mechanical Structures, School of Aerospace Engineering, Xi'an Jiaotong University, Xi'an 710049, China
[b] The George W. Woodruff School of Mechanical Engineering, Georgia Institute of Technology, Atlanta, GA 30332, USA
[c] CAS Key Laboratory of Nanosystem and Hierarchical Fabrication, National Center for Nanoscience and Technology, Beijing 100190, China

ARTICLE INFO

*Article history:*
Received 30 January 2017
Received in revised form 14 July 2017
Accepted 22 August 2017
Available online 6 September 2017

*Keywords:*
3D printing
Digital light processing
Conductive polymer composites
Sensors
Shape memory polymers

ABSTRACT

3D printing has gained significant research interest recently for directly manufacturing 3D components and structures for use in a variety of applications. In this paper, a digital light processing (DLP®) based 3D printing technique was explored to manufacture electrically conductive objects of polymer nanocomposites. Here, the ink was made of a mixture of photocurable resin with multi-walled carbon nanotubes (MWCNTs). The concentrations of MWCNT as well as the printing parameters were investigated to yield optimal conductivity and printing quality. We found that 0.3 wt% loading of MWCNT in the resin matrix can provide the maximum electrical conductivity of 0.027S/m under the resin viscosity limit that allows high printing quality. With electric conductivity, the printed MWCNT nanocomposites can be used as smart materials and structures with strain sensitivity and shape memory effect. We demonstrate that the printed conductive complex structures as hollow capacitive sensor, electrically activated shape memory composites, stretchable circuits, showing the versatility of DLP® 3D printing for conductive complex structures. In addition, mechanical tests showed that the addition of MWCNT could slightly increase the modulus and ultimate tensile stress while decreasing slightly the ultimate stretch, indicating that the new functionality is not obtained at the price of sacrificing mechanical properties.



## 1. Introduction

3D printing, or additive manufacturing (AM), has become increasingly popular, as it can be used to produce complex objects directly from digital files, such as CAD drawings. Along with the rapid development of 3D printing technologies, interest in using 3D printing to manufacture functional complex 3D structures has also grown significantly in the areas of biological applications [1,2], electronics [3,4], wearable device [5,6], shape memory polymer (SMP) devices [7], soft robots [8], and chemical applications [9]. Conductive materials are one of the most important subsets of 3D printed functional materials, due to their potential use as electrodes and connecting wires for signal transfer, heating as well as sensing. For instance, there is a critical need to develop printable conductive materials that can be either 3D printed or combined with 3D printed parts to address the need for 3D printable complex structures with multiple functions. In addition, new flexible printing platforms may need to be developed in order to meet the requirement of new conductive materials [10].

To address these needs, fabricating conductive structures using 3D printing technologies have been studied intensively in recent years. Hybrid printing, where two or more 3D printing technologies are integrated together, is one of the most common ways to print conductive structures within an electrically insulating material. For example, MacDonald's group [11,12] integrated direct printing technologies with stereolithography (SLA) and fused filament fabrication (FFF) to fabricate 3D electronics. Inkjet printing was also used to print conductive materials onto 3D printed substrates to fabricate conductive structures [7,13]. 3D printing porous structures and then impregnated them with conductive ink [14–16] can be used to obtain conductive structures. Recently, we integrated PolyJet 3D printing and direct ink writing (DIW) of silver traces to fabricate fully printed flexible sensors [6]. In these methods, the 3D printing process needs to be interrupted or paused to insert a second printing technology. In this way, fabricating intrinsically conductive 3D structures by directly 3D printing the conductive material becomes attractive. For example, past studies have examined polymer-based nanocomposite materials for 3D printing electrically conductive

* Corresponding authors.
*E-mail addresses:* qih@me.gatech.edu (H.J. Qi), wangtj@xjtu.edu.cn (T. Wang).
[1] These two authors have made equal contributions to the paper.

http://dx.doi.org/10.1016/j.addma.2017.08.011
2214-8604/

polymer composites through melt mixing [17–19], solution processing [20–22], and in situ polymerization [23,24].

Among the various 3D printing approaches, the digital light processing (DLP®) method using photocurable resins is attractive, because it can be used to fabricate a single layer of the 3D object through spatially-controlled solidification by using a projector light (either UV or white-light). In this way a layer can be formed rapidly [25]. In addition, it is possible to tailor the final properties of the printed object by simply changing the photocurable resin formulations [26]. By doing so, it is possible to achieve a large variety of systems for the production of structures with advanced properties and functions [23]. DLP® printable photocurable resin containing CNT fillers [27] or in situ generated silver nanoparticles [23,24] with enhanced electrical properties have been developed to 3D printing conductive structures. Incorporating electrically conductive fillers into photocurable resins for DLP® printing of 3D electrically conductive complex structures and device with multiple functions are still need constant effect to meet specific requirements in various applications.

Multi-walled carbon nanotubes (MWCNTs) have great potential for wide applications in structural materials and biomedical devices [28], and they can be used as fillers to polymer matrix for fabricating conductive composites [4,20]. In this paper, we present our recent progress on using the DLP® 3D printing method to manufacture 3D conductive complex structures by incorporating MWCNTs into photocurable resin. This paper is arranged as follows. We first introduce the materials and experimental methods. We then show various 3D printed conductive structures. By studying conductivity, viscosity and scanning electron microscopy (SEM) images, we identify optimized MWCNT concentration and printing parameters. We further investigate the electrical performance of printed MWCNT nanocomposite structures as sensors, SMP composites and stretchable electrical circuits. Finally, we study the mechanical properties and thermal stability of printed MWCNT nanocomposites.

## 2. Materials and methods

### 2.1. Materials

A commercially available acrylic based photocurable resin (Are3d-dlp405, TMTCTW, Fuzhou,Fujian, China) was used as the matrix material of the nanocomposites, according to the supplier, this brand resin has different colors which only caused by additive of different colored pigment, we used orange and yellow color resin in this work. MWCNTs (FloTube™ 7000, CNano Technology Ltd., Beijing, China) fabricated from a chemical vapor deposition process with a purity >93 wt% were used as the filler material for the nanocomposites. The dimensions of the MWCNTs were 6–8 nm in diameter and up to 50 μm in length. Dimethylformamide (DMF, Sigma Aldrich, Shanghai, China) and Triton x-100 (Sigma Aldrich, Shanghai, China) were used as received to disperse the MWCNTs.

### 2.2. Experiments

#### 2.2.1. MWCNT nanocomposites preparation

To prepare the MWCNT nanocomposite material, two typical mechanical dispersion techniques, ultrasonication and ball mill, were used to disperse the MWCNTs [28]. We used an ultrasonic dispersion method to prepare small quantities of the nanocomposite material with various MWCNT concentrations. This method was used to measure conductivity and viscosity and to optimize the MWCNT loading. After magnetically stirring a combination of Triton x-100 and DMF at 1200 rpm for 5 min (RCT, IKA, Sigma Aldrich, Shanghai, China), the desired amount of MWCNTs was dispersed in the DMF/Triton x-100 solution by a sonifier (JY99-IID, Ningbo Xinzhi Biotechnology Ltd., Ningbo, Zhejiang, China) for 2 h at 20 kHz (900 W, oscillation amplitude 50%). This mixture was then added to the photocurable resin and was ultrasonically dispersed for another 2 h, using the same operating conditions as above. Finally, the MWCNT/DMF/resin mixture was placed into a vacuum oven with the pressure of 5 kPa (DZF-6050, Shanghai Yiheng Instruments Co., Ltd., Shanghai, China) at 50 °C for 1 h to remove the DMF solvent.

After finding the optimized MWCNT loading (0.3 wt%), we used a three-roll milling method to fabricate large quantities of the MWCNT nanocomposites that were used for DLP® 3D printing with the specific MWCNT content. Here, a specific quantity of MWCNTs was mechanically mixed with the photocurable resin in a high-speed mixer (Dispermat AE, VMA-Getzmann GmbH, Germany) for 30 min at 3000 rpm and then twice processed in a three-roll mill (Exakt 80E, EXAKT Technologies, Inc., Germany) by spacing mode (75 μm:25 μm, 30 μm:10 μm, 15 μm: 5 μm) and a rolling speed of 100 rpm in order to get a homogeneous dispersion of MWCNT fillers in the resin matrix. Once dispersed, the solution could be held at a colloidal state for a prolonged period of time (at least three months) such that no MWCNT sedimentation was observed in the unused solution. The nanocomposite was stored in a dark area before being used for printing.

#### 2.2.2. DLP® printing of complicated structures use MWCNT nanocomposite

A modified (sweeper was removed) commercial 3D printer, B9Creator (V1.1, B9Creations, LLC, Rapid City, SD, USA), was used in this study (as Fig. 1a). B9Creator is a bottom-up DLP® printing system (Fig. 1b) where the light source from a projector is focused on the bottom surface of the resin vat during printing. A motorized building platform is mounted above the resin vat. A layer is first polymerized between the bottom of the vat and the surface of the build platform by the projector light projecting a cross-sectional image of the desired planar geometry for a predefined time (Fig. 1c ①). Once one layer is cured, the light source is turned off and the resin vat shifts horizontally (in the x-axis) to shear off the printed part from the bottom of the resin vat (Fig. 1c ②). After shearing, the build platform moves up by a specified distance d to form a small gap between the printed object and the bottom surface of the resin vat, allowing new resin to fill into the projection area (Fig. 1c ③). The vat then returns to the projection area, and the build platform moves down a distance of d-$d_T$ (where $d_T$ is the layer thickness); then a uniform thin layer can be achieved after the formed gap is fully filled with resin (Fig. 1c ④) [29]. This process is repeated in a layer-by-layer manner until the final 3D geometry, defined by a CAD model, is achieved. After printing, the part is removed from the platform and washed with ethanol, resulting in a completed part. A polarized microscopic image in Fig. 1d shows the stacked layers from a cross sectional view of the printed object.

In order to print structures with multiple materials (various colors and electrical properties), we follow the method by Ge et al. [26], where separate resin vats were used and loaded with different prepared resins. After printing a specified number of layers using a certain material, the printer was paused, the vat was changed to a secondary material, and the printing was resumed, by using this method we can print multiple materials within one layer at cost of printing speed. To print hang structured spring, we printed supporting pillars that can be easily removed with a razor blade after printing.

#### 2.2.3. Electrical characterization

*2.2.3.1. Resistivity.* A sourcemeter (Keithley 2400, Tektronix Inc., Shanghai, China), controlled by its own data acquisition program (LabTracer 2.0), was used to measure and record the resistance of the printed samples. For all resistance measurements, a two-point probe method was used to calculate the bulk resistivity and

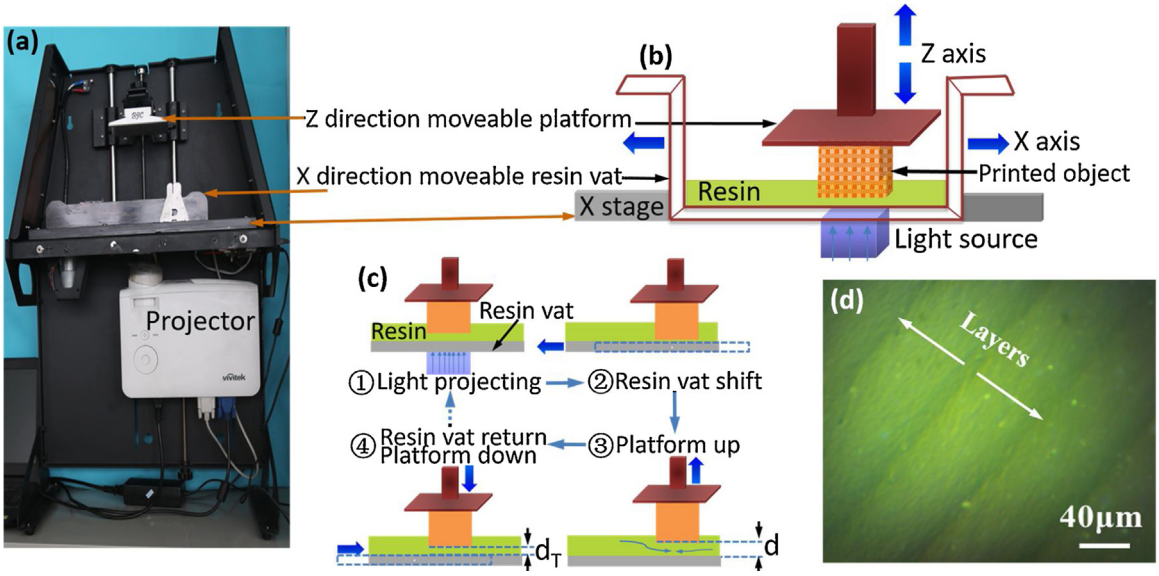


**Fig. 1.** (a) B9Creator 3D printer (without sweeper). (b) Schematic of DLP® printing system. (c) Schematic illustration of printing process, Note: schematics not drawn to scale. (d) A microscope image of printed object's cross section.

the resistance change during mechanical deformation tests. The resistivity of the printed strips was calculated as

$$\rho = \frac{R \cdot A}{l}, \tag{1}$$

where $R$ is the measured resistance, $l$ is the distance between terminals, and A is the cross-section area of the printed structure.

*2.2.3.2. Ohmic heating.* A Keithley 2400 sourcemeter was used to heat partially conductive printed structures by passing an electrical current through the MWCNT nanocomposite areas. An infrared video camera (NS9500PRO, NEC Avio, Japan) was used to record the infrared images during electrical heating at a frequency of 1 Hz. Resistive heating within the printed resistor can be expressed by Joule's law as:

$$Q = I^2Rt, \tag{2}$$

where $Q$ is the heat transferred in Joules, $I$ is the applied current, $R$ is the resistance within the electric circuit, and t is the time the circuit is active.

*2.2.3.3. Capacitance.* Capacitance was measured by using an LCR meter (3532-50 LCR HiTESTER, HIOKI, Japan) and was recorded using a data acquisition program provided by the manufacturer. For the compression experiments conducted on the hollow structured capacitive sensor, an electromechanical test frame (AGS-X, Shimadzu, Japan) was used to apply the mechanical loading, and the capacitance changes were measured and recorded at 20 kHz. For the liquid level experiment, a certain amount of liquid (about 0.2 mL–0.8 mL) was inserted into the hollow capacitive sensor by using a tilted syringe from any one of the hole, and the capacitances were measured at 5 kHz.

*2.2.4. Mechanical testing*

Tensile tests of the printed pristine resin specimens and MWCNT nanocomposite specimens were conducted using the AGS-X electromechanical testing frame equipped with a laser extensometer. The crosshead speed was 1 mm/min. Dog bone specimens with a gage length of 10 mm were printed. At least three specimens made under each printing condition were tested to obtain stress-strain curves and to determine tensile strength, elongation and Young's modulus.

*2.2.5. Other characterization techniques*

The apparent viscosities of pristine resin and MWCNT/resin mixture were measured with a viscometer (NDJ-9S, Shanghai Pingxuan Scientific Instruments Co., Ltd., Shanghai, China). The measurements were carried out at 6, 12, 30 and 60 revolutions per minute (RPM) under the ambient condition (about 25 °C). To investigate the microstructure of the MWCNT nanocomposites, scanning electron microscopy (SEM, JSM-7500F, JEOL Ltd., Japan) images were taken with an accelerating voltage of 5 kV. The FTIR spectra (supporting information Fig. S1) of MWCNT nanocomposites before printing and after DLP® printing were scanned by spectrometer (Tensor 27, Bruker, Germany) with attenuated total reflectance (ATR) module. The glass transition behavior of the MWCNT nanocomposite was tested on a DMA tester (Model Q800, TA Instruments, New Castle, DE, USA) in tensile mode, the temperature was increased from 0 °C to 120 °C at a rate of 2 °C/min. Cross-sectional images of printed structures were taken with a polarizing microscope (BK-POL, OPTEC, Chongqing, China). Thermogravimetric analysis (TGA, TG209C, NETZSCH, Bavarian, Germany) was conducted between 40 °C and 900 °C at a heating rate of 10 °C/min to compare the thermal stability of printed pristine resin and MWCNT nanocomposite (Fig. S3).

## 3. Results and discussion

### 3.1. DLP® *printed MWCNT nanocomposite conductive complex structures*

By adjusting the printing parameters, planar and complex 3D structures with single or multiple materials were printed as shown in Fig. 2. Here, we display the capability of printing planar structures, hanging and hollow structures and structures composed of more than one material. We printed a spring (Fig. 2a), a wave shaped resistor (Fig. 2b), and a truss (Fig. 2c) using MWCNT nanocomposite, as well as a hollow capacitive sensor using MWCNT nanocomposite as electrodes (Fig. 2d). By using the two-vats approach, we printed capacitors (Fig. 2e and f) using pristine resin as a dielectric layer and the MWCNT nanocomposite as the electrodes. We also printed resistors (Fig. 2g and h) with orange-color pristine resin, yellow-color pristine resin, and MWCNT nanocom-

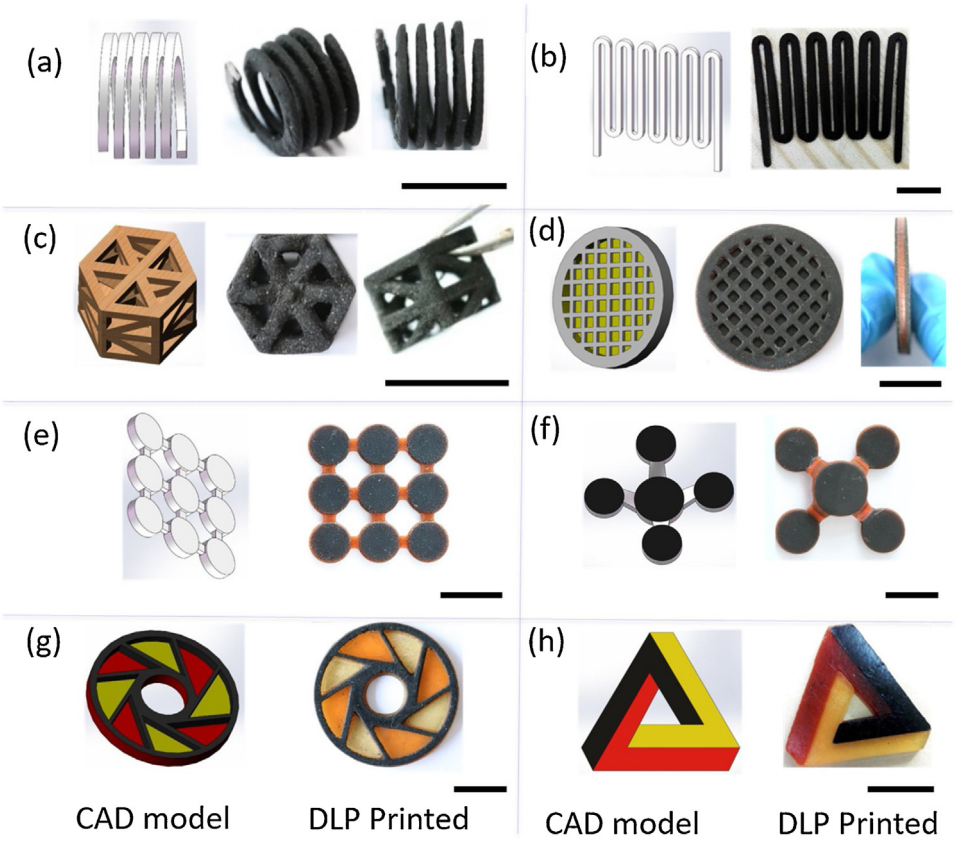


**Fig. 2.** Different types of DLP® 3D printed conductive structures with MWCNT nanocomposite and pristine resins according to designed CAD models which are shown at the left side of the printed objects: objects in (a)–(c) printed only by MWCNT nanocomposite (a) hang structured spring; (b) planar wave shape resistor; (c) hollow structure truss. Structures in (d)–(f) printed with two types of materials which used MWCNT nanocomposite and pristine resin, (d) capacitor with hollow structure, (e) capacitor array, (f) capacitors at different heights. Structures in (g), (h) printed with three types of materials, (g), (h) partially conductive structures printed by MWCNT nanocomposite, pristine orange resin and pristine yellow resin. Scale bar for printed objects is 10 mm.

posite. These structures were printed based on the optimized printing parameters, as will be discussed below.

### 3.2. Optimization of MWCNT loading and DLP® printing parameters

Due to the introduction of MWCNTs into the photopolymer resin, the physicochemical properties of the 3D printing ink change. It is therefore necessary to study the processing parameters that lead to the best printing quality and to optimized electrical properties. Here, we first studied the effects of the MWCNT loadings on the conductivity of the printed materials. The electrical conductivity of the printed MWCNT nanocomposite structures was measured using the common two-point probe method, and the results are shown in Fig. 3a. With a concentration of the MWCNT <0.1 wt%, the nanocomposite was not conductive. The samples gained electrical conductivity at a loading around 0.1 wt%, indicating that the conductive percolation had begun to form. The conductivity then showed a significant increase with the increase in MWCNT concentrations and reached 0.027 S/m at 0.3 wt%, after which the rate of increase slowed. The conductivity of our DLP® printed MWCNT nanocomposites is reasonable as compared to values obtained in other works [27,30]; in addition, the nanocomposites prepared by ultrasonic dispersion and by the three-roll milling method are in same order of magnitude, indicating they have similar conductivity. From the inset images we can see that the dispersed MWCNTs alter the optical properties of the resin, changing from clear to opaque, and consequently affecting the transmittance of the resin. Because of this change in transmittance, the exposure time of DLP® printing should be increased with the increase of MWCNT loading, FTIR spectra (Fig. S1) were used to characterize the photocuring to make sure the peak of acrylate double bonds at 1640 $cm^{-1}$ nearly disappeared.

The apparent viscosity as a function of MWCNT concentration and shearing rate is shown in Fig. 3b. The viscosity increases as the loading of MWCNT increases, and it exhibits a shear thinning response. As mentioned in the experimental section, during DLP® printing, the resin needs to be refilled into the small gap between the printed object and the bottom surface of the resin vat to form a thin layer as shown in Fig. 1c ③. If the viscosity is too high, it limits the material's ability to flow and leads to air bubble formation within the printed part. Therefore, the loading ratio of MWCNT fillers was chosen such that it yielded a highly conductive nanocomposite while maintaining the viscosity low enough to enable the material to flow during DLP® printing. Since maximizing conductivity is always desirable, we found that a MWCNT concentration of 0.3 wt% (with viscosity of about 10 Pa s at 6 RPM, similar to 11.5 Pa s at a shear rate of 1 $s^{-1}$ of 0.3 wt% CNTs filler in other work [27]) is suitable for good DLP printing quality as well as good conductivity. We also studied the effect of the processing parameters on the mechanical properties of the DLP® printed parts. Based on our experience (results not shown), for the 0.3 wt% MWCNT nanocomposites, a layer thickness of 19.05 μm and an exposure time of 40 s provided the best mechanical properties, compared to pristine resin with a layer thickness of 31.75 μm and exposure time of 8 s. The SEM image of 0.3 wt% MWCNT nanocomposite is shown in Fig. 3c, which displays the good distribution of white spots, corresponding to MWCNTs.

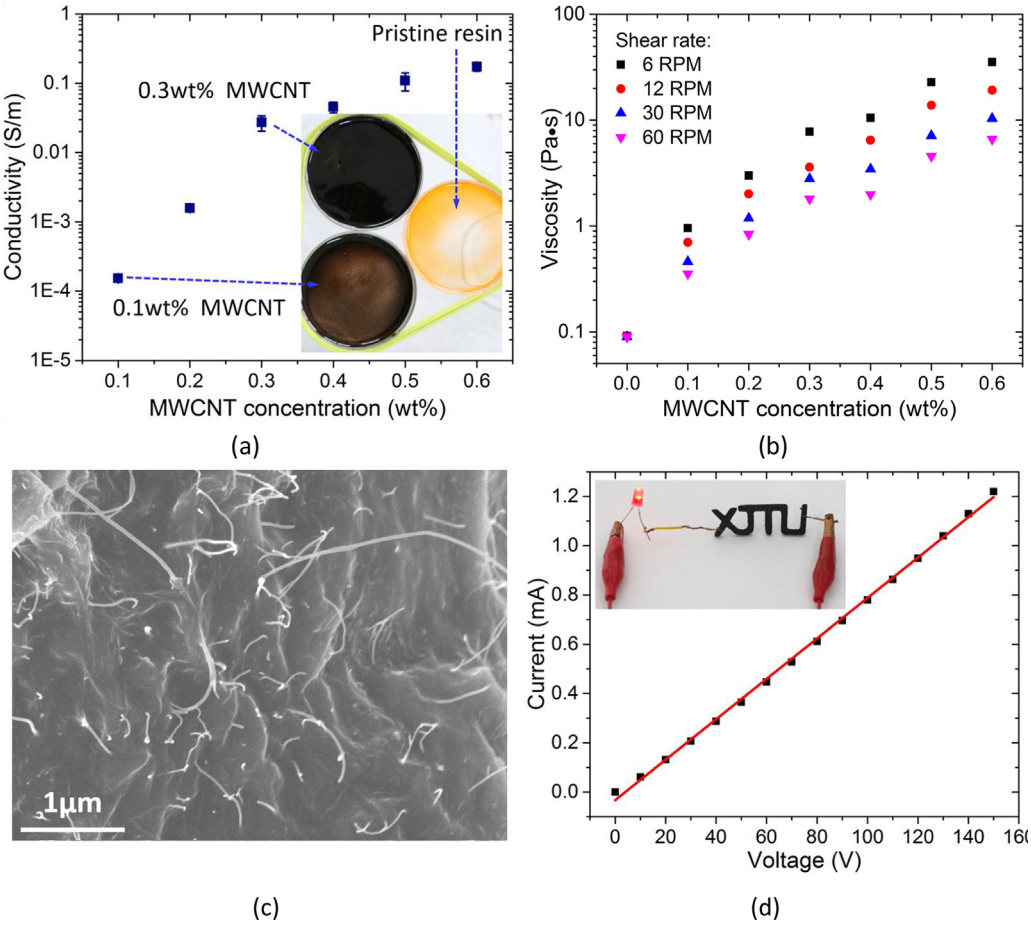


**Fig. 3.** (a) Conductivity as function of MWCNT loading; inserted optical images are of same volume pristine resin and MWCNT nanocomposites in the same types of watch glass. (b) Apparent viscosity as a function of MWCNT loading and shear rate. (c) SEM image of printed MWCNT nanocomposites with 0.3 wt% MWCNT loading. (d) I–V curve of printed 0.3 wt% MWCNT nanocomposite resistor, inset shows the resistor connecting to 3 V voltage source and LED.

Fig. 3d shows the I–V curve of the printed MWCNT nanocomposite resistor. The linearity of the curve indicates a stable conductivity and a purely resistive element. The LED can be illuminated by applying 3 V to a circuit with a printed resistor connected in series with the LED.

### 3.3. Electrical performance of DLP® printed electronic devices

In this section we evaluate the electrical performance of some selected structures in Fig. 2, in order to provide a better understanding of the performance of DLP® 3D printing with a MWCNT nanocomposite resin for fully printed complex conductive structures.

#### 3.3.1. Hollow structured capacitive sensor

By using the electrical performance of MWCNTs, we were able to fabricate a fully 3D printed capacitive sensor as shown in Fig. 2d, where the top electrode was designed with a network shape. Fig. 4a shows schematically the cross-sectional drawing of the capacitive sensor with a hollow structure; both the network electrode and the hollow structure designs were used to allow the sensor to be easily deformed. The capacitance $C$ of two parallel plates is given by:

$$C = \frac{\varepsilon_0 \varepsilon_r A}{d}, \tag{3}$$

where $\varepsilon_0$ is the free space permittivity, $\varepsilon_r$ is the relative permittivity of the dielectric medium, $A$ is the effective surface area, $d$ is the spacing between electrodes. From Eq. (3), we can see that the capacitance increases when the distance between the two plates decreases or when the permittivity of the dielectric medium between the plates increases. Following this principle, the fully 3D printed sensor can be used to detect changes in the spacing between the two plates; this enables it to sense compressive strain or forces, as shown in Fig. 4a-II, or changes in the level of a liquid (Fig. 4a-III).

The ability of the fully printed hollow capacitive sensor to detect strain or force was tested as described in the experimental part. Here the strain is the nominal strain, defined as the displacement divided by the original thickness of the capacitor. As shown in Fig. 4b, the capacitance dependence on strain up to 70% of nominal strain was tested. The repeatability of the capacitor sensor was also measured, and the results are shown in Fig. 4c, where the sensor was subjected to a cyclic compression test for six cycles with a deformation velocity of 14 mm/min to 60% strain and holding for 6 s. It can be seen that the capacitive sensor is repeatable. Figs. 4d and e show the capacitance change with pressure (which is defined as the force applied to compress the top surface divided by the top surface area), also with reasonable repeatability and sensitivity.

Capacitive sensors have been used for liquid-level measurements [31,32] previously. Fluidic valves and pumps were printed within microfluidic devices using the SLA technique at a low cost for lab-on-chip devices [33]. The mechanism of such a capacitor is shown in Fig. 4a-III. When a non-conductive liquid is added to the hollow cavity of a capacitor, changing the medium will change the permittivity of the dielectric and thus the capacitance. This allows the creation of a capacitive sensor that detects the change in liquid levels. Here, we show the potential of printing a sensor

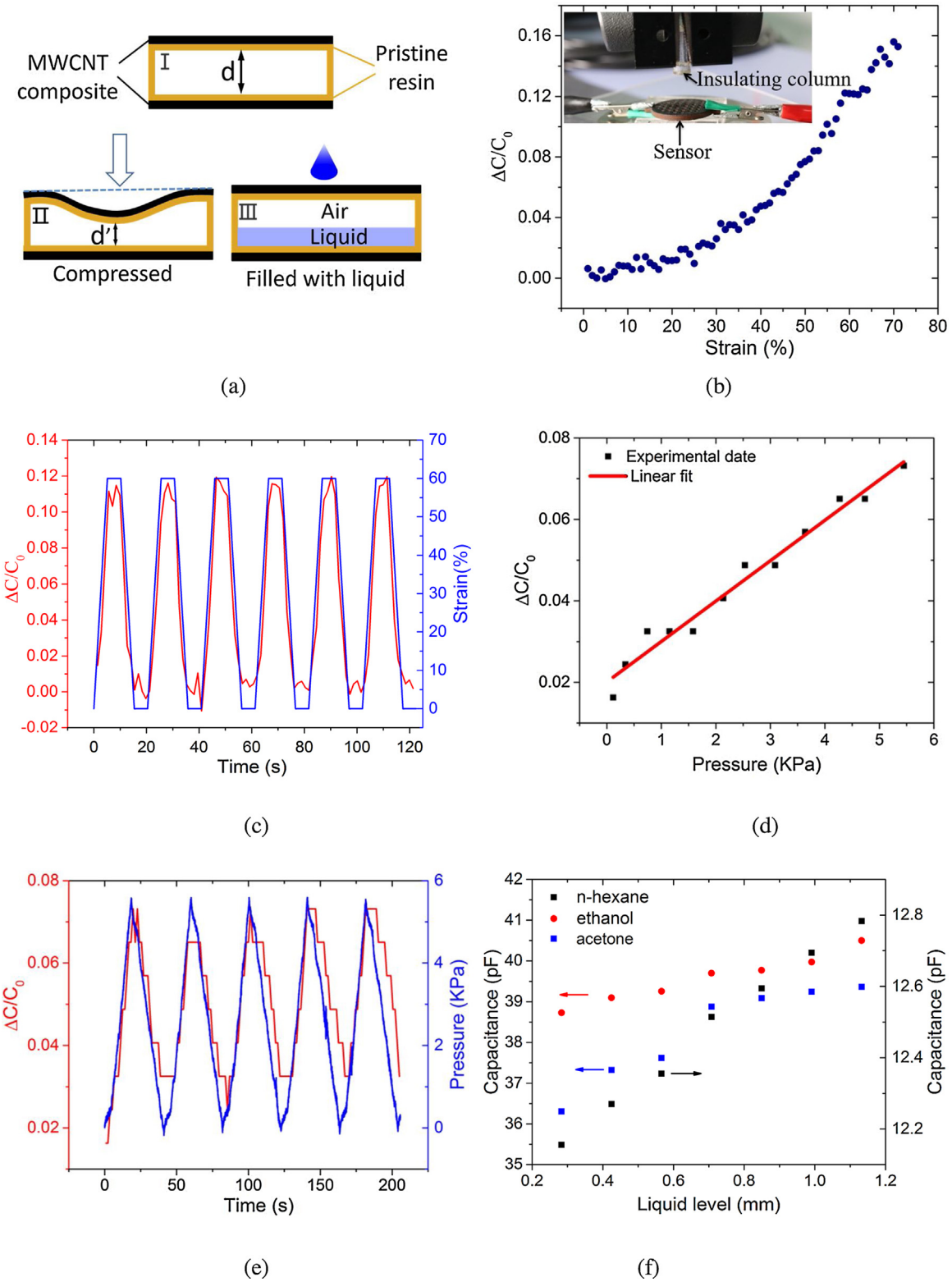


**Fig. 4.** DLP® printed MWCNT nanocomposite hollow capacitive sensor (Fig. 2d): (a) The schematics are the sectional drawing of the capacitive sensor (I), when compressed (II) and filled with liquid (III). (b) Change in capacitance $\Delta C/C_0$ versus with strain $\varepsilon$, the inset view shows capacitor between two clamps, an electrically insulating column attached to one clam to apply the load. (c) $\Delta C/C_0$ versus time t over 6 cycles of applied pressing. (d) Change in capacitance $\Delta C/C_0$ versus with pressure. (e) $\Delta C/C_0$ versus time t over 5 cycles of applied pressure. (f) Capacitance as a function of filled liquid level and type of liquid.

for liquid level detection. We filled the above mentioned hollow structured capacitive sensor (Fig. 2d) with different kinds of liquid, such as ethanol, acetone and *n*-hexane, which have dielectric constants of 24, 20 and 1.58 respectively, and different volumes (or different heights). From Fig. 4f we can see that the capacitance C increases with the increase of liquid level that caused by increased liquid volume. In addition, when filled to the same liquid level, the ethanol and acetone filled capacitors show a larger capacitance than

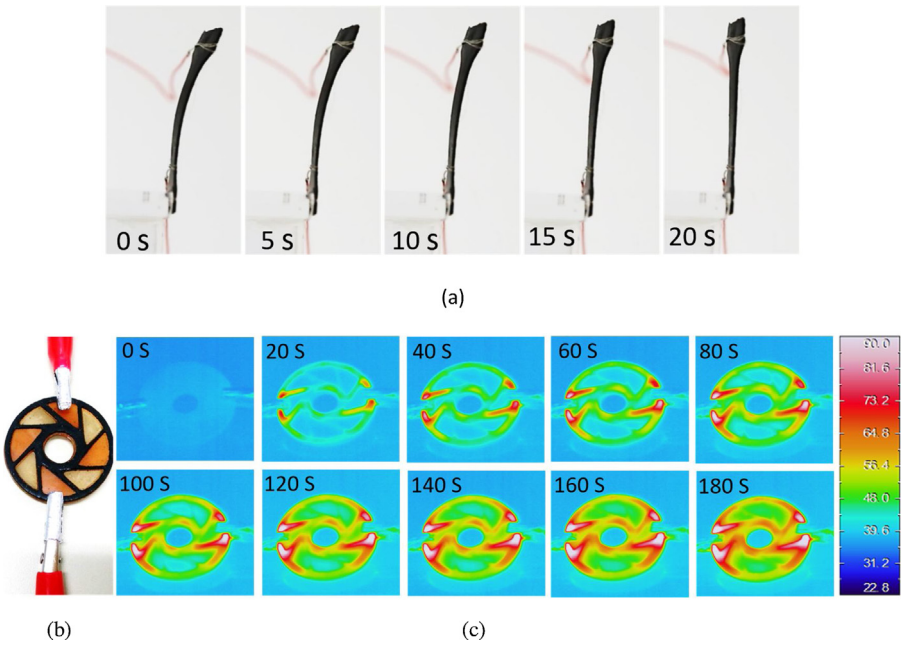


**Fig. 5.** (a) Shape memory effect of a DLP® printed MWCNT nanocomposite strip: shape change of the sample during ohmic heating (by 180 V voltage). Snapshot of Joule heating induced temperature increase recorded by infrared video camera (b) optical image (Fig. 2g), (c) infrared images during heating.

that of the *n*-hexane capacitor. This is consistent with the fact that ethanol and acetone have larger dielectric constants than *n*-hexane. The DLP® printing technology provides a fast way to create a sensor array in an integrated system to enable the detection of force, strain, and liquid level change. We demonstrated the feasibility of this method here; however, for practical application, many other issues, such as long term performance, repeatability, etc., need to be addressed.

### 3.3.2. Shape memory effect stimulated by ohmic heating

The ability to fabricate SMP devices with complicated geometry is important for soft robotics, flexible electronics, medical devices, and other areas [7]. Usually, the SMP is firstly deformed at a high temperature (usually above the glass transition or melting point) and subsequently frozen upon cooling to fix the programmed temporary shape [34]. Here, we demonstrate potential applications of DLP® printed MWCNT nanocomposites with shape memory effect induced by ohmic heating and localized heating of the structures. To demonstrate the shape memory behavior of the DLP® printed nanocomposite, we performed a full shape memory cycle; we first heated (by hotplate or ohmic heating) the printed strip to 65 °C (above $T_g$ of 36 °C in Fig. S2) to deform the strip. After lowering the temperature and being fixed into a temporary shape, the bent strip was connected to a 180 V electrical circuit; it then fully recovered to its original shape in 20 s due to ohmic heating as shown in Fig. 5a.

Additionally, we use the structure in Fig. 2g, in which only the black color portions are conductive, to show that printed conductive nanocomposites can be designed to have local heating zones. Infrared (IR) thermographs of the printed partially conductive structure (Fig. 2g) at constant current of 3.0 mA are shown in Fig. 5c. As ohmic heating occurred, at 0.45W of input power, the temperature of the MWCNT nanocomposite parts rose gradually to about 80 °C in two minutes, but the temperature of the pristine resin parts remained nearly constant. The steady state temperature and settling time can be adjusted by the input power. In general, a larger input power corresponds to shorter heating time and higher heated temperature.

### 3.3.3. High strain sensitive capability

CNT based composites are considered to be a realistic alternative to conventional smart materials [35,36] and there is great interest in fabricating highly sensitive strain sensors with MWCNT composites [37,38]. Our DLP® printed MWCNT nanocomposites also exhibit strain sensitive behavior. We conducted strain sensitive measurements. The strain of the specimen was recorded using a laser extensometer, while the resistance of the MWCNT nanocomposite was simultaneously measured using a Keithley 2400 sourcemeter. Fig. 6a shows that the resistance increases in a linear manner up to 2% strain. As the application of strain sensing often requires reversible strain loadings, MWCNT nanocomposite was subjected to cyclic strain profiles as in Fig. 6b; it is noted that the resistivity changes in the same manner as the strain changes. In addition, the resistivity peak shows a slight decrease after 3 cycles; however, it almost stabilizes in the following cycles. Meanwhile, to minimize the contact resistance [39] is also needed. Strain sensitivity is one of the key performance indicators for strain sensing materials. The sensitivity magnitude is commonly referred to as the gauge factor, *s*, which is defined by

$$s = \frac{\Delta R/R_0}{\varepsilon} \tag{4}$$

where $\Delta R$ is the resistance change, $R_0$ is the initial resistance, and $\varepsilon$ is the strain. As the fitted curve in Fig. 6a, our printed MWCNT nanocomposite has a gauge factor of 38; this is high as compared to some previous works [40], indicating that our MWCNT nanocomposite has a high sensitivity and thus can be used as a smart material for strain sensing. The MWCNT nanocomposite can be repeated for about 10 cycles at a strain of 2.5%. For long time repeatability, the mechanical properties such as ductility of the nanocomposite should also be taken into consideration.

### 3.3.4. Stretchable circuit

Stretchable electronics have drawn considerable research attention recently [41]. A variety of methods, including wavy or serpentine structures [42], intrinsically stretchable materials [43], and a combination of intrinsic and design-induced stretchability [44], have been widely used. CNTs have been widely used to fabri-

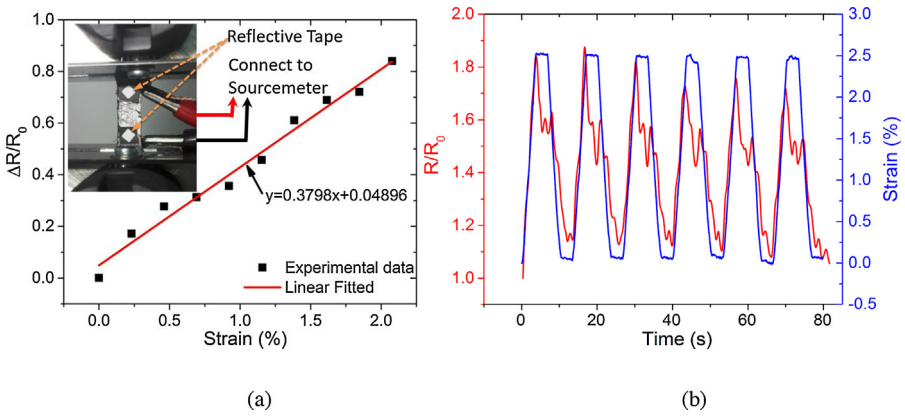


**Fig. 6.** (a) Normalized resistance change during stretching, the inserted image shows the measuring set-up for strain sensitive testing of MWCNT nanocomposite. (b) Normalized resistance change and cyclic strain profile of MWCNT nanocomposite for 6 cycles.

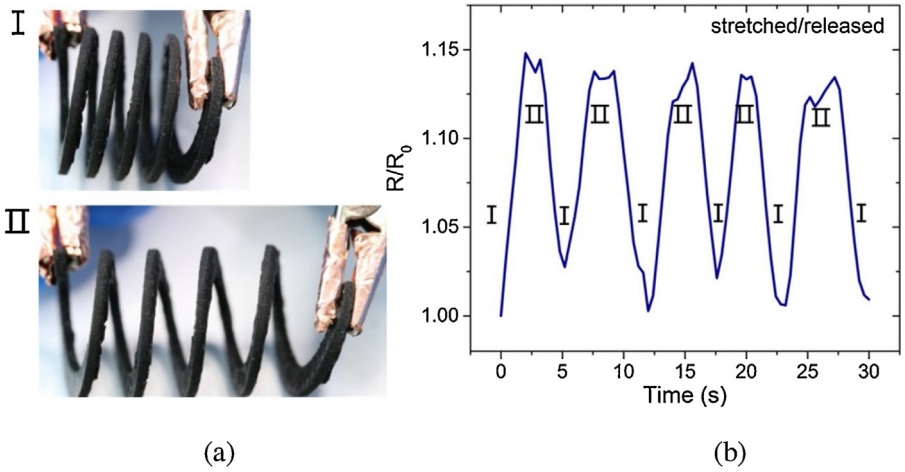


**Fig. 7.** Printed spring as stretchable circuit: (a) Images of a stretchable spring structure in released (I) and stretched (II) positions. (b) Change in resistance of a representative gauge during five stretching/releasing cycles.

cate CNT-based stretchable conductors [45,46]. Taking advantage of the merit of DLP® 3D printing and based on design-induced stretchability [44], we printed a free standing stretchable spring structure (Fig. 2a) using MWCNT nanocomposite. The stretchable spring was manually tested in stretched/relaxed configurations, and the resistance change was measured using a Keithley 2400 sourcemeter. As shown in Fig. 7a, the spring can be stretched by as much as 100%. When stretched, the resistance increased; when returned to the relaxed position, the resistance dropped; the typical operating response can be seen in Fig. 7b. From Fig. 7 we can see that when the spring is stretched to about twice the original length the resistance only increases about 13%, and the resistance nearly recovered to the original value when the spring returned to the relaxed position. Therefore, the DLP® printed spring structure can be used as a stretchable interconnect and can be integrated in all printed stretchable electronic devices.

### 3.4. *Mechanical properties of DLP® **printed objects***

The mechanical properties of MWCNT nanocomposites were tested by tensile testing. Fig. 8a shows the stress strain curves of printed pristine resin and 0.3 wt% MWCNT nanocomposite. The comparison of modulus, ultimate tensile stress and ultimate elongation at break are summarized in Fig. 8b. Young's modulus was calculated by linear regression at the slope between 0.5% in the stress vs. tensile strain curves. We can see that the ultimate tensile stress and modulus of the MWCNT nanocomposite are increased by 21% and 45% respectively, compared to the pristine resin, while the elongation at break decreased about 10%. These results indicate that overall the mechanical properties remain the same as the pristine resin. The SEM images of a fracture surface in Fig. 8c show noticeable differences between the pristine resin and the MWCNT nanocomposite samples. The pristine resin sample has a smooth surface compared to the MWCNT nanocomposite sample, which has a very coarse surface. The interface layer for the pristine resin sample can be seen clearly; the white segments in the SEM images of the MWCNT nanocomposite sample represent the ends of MWCNTs in the fracture surface. Voids and grooves can also be observed on the fracture surface's coarse area, corresponding to the locations where the MWCNTs were completely pulled out and indicating in some areas a weak interface between the MWCNTs and the matrix. This might be because light cannot penetrate through the resin completely, leaving some places where the resin cannot be fully cured. One way to remedy this drawback is to further reduce the layer thickness, but this will increase the printing time.

## 4. Conclusions

In the paper, we demonstrated the ability to use DLP® 3D printing to fabricate complex conductive structures from a material made of dispersed MWCNTs in a photocurable resin. Considering both electrical conductivity and printability, the best MWCNT

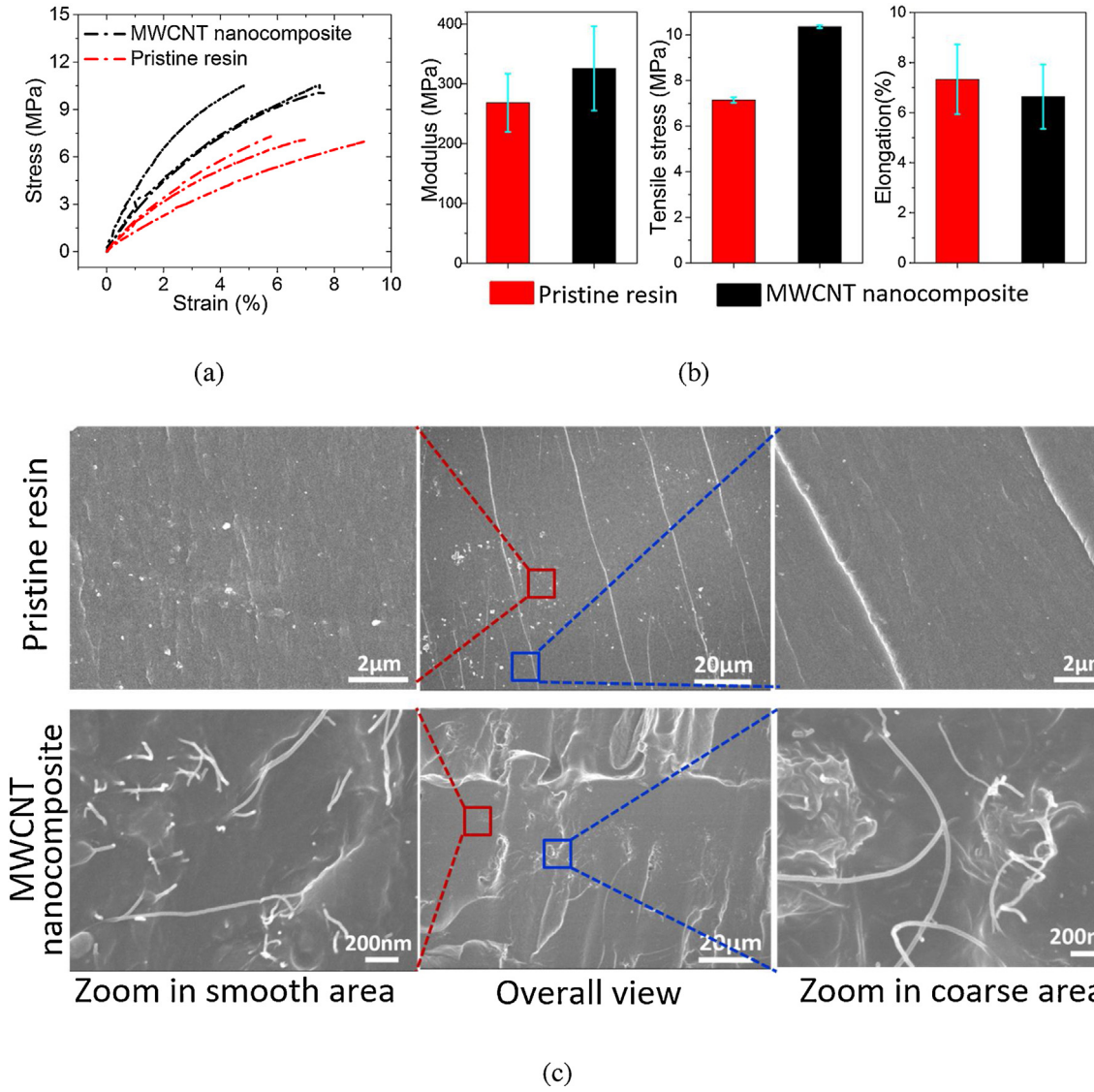


**Fig. 8.** (a) Comparison of stress-strain curves of printed pristine resin samples with printed 0.3 wt% MWCNT nanocomposite samples. (b) Comparison of modulus, ultimate tensile stress and elongation of printed pristine resin samples and printed 0.3 wt% MWCNT nanocomposite samples. (c) SEM images of fracture surface of pristine resin sample and 0.3 wt% MWCNT nanocomposite sample.

loading was found to be 0.3 wt% with the printing parameters of 19.05 μm layer thickness and light irradiation time of 40 s. The printed complex structures have reasonably good electrical properties. We also demonstrated the potential application of DLP® printed conductive complex structures as hollow capacitive sensors, smart structures with shape memory effects, partially conductive structures and stretchable spring circuits. These demonstrations indicated several possibilities in the design and fabrication of geometrically complex structures with tailored electrical performances by balancing a fast, cost effective and versatile production process with the promising final functionality of the printed structures.

## Acknowledgements

T.W. acknowledges financial support from National Natural Science Foundation of China (grant NSFC 11272246). HJQ and CKD acknowledge support from the US Air Force Office of Scientific Research (grant FA9550-16-1-0169; Dr. B.-L. "Les" Lee, Program Manager) and the US National Science Foundation (grant CMMI-1462895).

## Appendix A. Supplementary data

Supplementary data associated with this article can be found, in the online version, at http://dx.doi.org/10.1016/j.addma.2017.08.011.

## References

[1] M.S. Mannoor, et al., 3D printed bionic ears, Nano Lett. 13 (6) (2013) 2634–2639.
[2] L.A. Hockaday, et al., 3D-printed hydrogel technologies for tissue-engineered heart valves, 3D Print. Addit. Manuf. 1 (3) (2014) 122–136.
[3] E. MacDonald, R. Wicker, Multiprocess 3D printing for increasing component functionality, Science 353 (6307) (2016), p. aaf2093.
[4] M. Vatani, E.D. Engeberg, J.-W. Choi, Conformal direct-print of piezoresistive polymer/nanocomposites for compliant multi-layer tactile sensors, Addit. Manuf. 7 (2015) 73–82.
[5] J.T. Muth, et al., Embedded 3D printing of strain sensors within highly stretchable elastomers, Adv. Mater. 26 (36) (2014) 6307–6312.
[6] Q. Mu, et al., Thermal cure effects on electromechanical properties of conductive wires by direct ink write for 4D printing and soft machines, Smart Mater. Struct. 26 (4) (2017) 045008.
[7] M. Zarek, et al., 3D printing of shape memory polymers for flexible electronic devices, Adv. Mater. (2015).

[8] M. Wehner, et al., An integrated design and fabrication strategy for entirely soft: autonomous robots, Nature 536 (7617) (2016) 451–455.
[9] K.B. Anderson, et al., A 3D printed fluidic device that enables integrated features, Anal. Chem. 85 (12) (2013) 5622–5626.
[10] J.O. Hardin, et al., 3D printing: microfluidic printheads for multimaterial 3D printing of viscoelastic inks (Adv. Mater. 21/2015), Adv. Mater. 27 (21) (2015) 3279–3284.
[11] E. Macdonald, et al., 3D printing for the rapid prototyping of structural electronics, IEEE Access 2 (2014) 234–242.
[12] C. Shemelya, et al., 3D printed capacitive sensors, in: Sensors, 2013 IEEE, IEEE, 2013.
[13] J. Kimionis, et al., 3D/inkjet-printed origami antennas for multi-direction RF harvesting, in: 2015 IEEE MTT-S International Microwave Symposium, IEEE, 2015.
[14] I. Cooperstein, M. Layani, S. Magdassi, 3D printing of porous structures by UV-curable O/W emulsion for fabrication of conductive objects, J. Mater. Chem. C 3 (9) (2015) 2040–2044.
[15] J. Czyzewski, et al., Rapid prototyping of electrically conductive components using 3D printing technology, J. Mater. Process. Technol. 209 (12) (2009) 5281–5285.
[16] X. Mu, et al., Porous polymeric materials by 3D printing of photocurable resin, Mater. Horiz. 4 (3) (2017) 442–449.
[17] S.J. Leigh, et al., A simple, low-cost conductive composite material for 3D printing of electronic sensors, PLoS One 7 (11) (2012) e49365.
[18] S.R. Athreya, K. Kalaitzidou, S. Das, Processing and characterization of a carbon black-filled electrically conductive Nylon-12 nanocomposite produced by selective laser sintering, Mater. Sci. Eng.: A 527 (10) (2010) 2637–2642.
[19] X. Wei, et al., 3D printable graphene composite, Sci. Rep. (2015) 5.
[20] G. Postiglione, et al., Conductive 3D microstructures by direct 3D printing of polymer/carbon nanotube nanocomposites via liquid deposition modeling, Compos. Part A: Appl. Sci. Manuf. 76 (2015) 110–114.
[21] R.D. Farahani, et al., Reinforcing epoxy nanocomposites with functionalized carbon nanotubes via biotin-streptavidin interactions, Compos. Sci. Technol. 72 (12) (2012) 1387–1395.
[22] J.M. Gardner, et al., 3-D printing of multifunctional carbon nanotube yarn reinforced components, Addit. Manuf. 12 (2016) 38–44.
[23] E. Fantino, et al., 3D printing of conductive complex structures with In situ generation of silver nanoparticles, Adv. Mater. 28 (19) (2016) 3712–3717.
[24] E. Fantino, et al., In situ thermal generation of silver nanoparticles in 3D printed polymeric structures, Materials 9 (7) (2016) 589.
[25] J.W. Stansbury, M.J. Idacavage, 3D printing with polymers: challenges among expanding options and opportunities, Dent. Mater. 32 (1) (2016) 54–64.
[26] Q. Ge, et al., Multimaterial 4D printing with tailorable shape memory polymers, Sci. Rep. (2016) 6.
[27] G. Gonzalez, et al., Development of 3D printable formulations containing CNT with enhanced electrical properties, Polymer 109 (2017) 246–253.
[28] P.-C. Ma, et al., Dispersion and functionalization of carbon nanotubes for polymer-based nanocomposites: a review, Compos. Part A: Appl. Sci. Manuf. 41 (10) (2010) 1345–1367.
[29] Y. Pan, C. Zhou, Y. Chen, A fast mask projection stereolithography process for fabricating digital models in minutes, J. Manuf. Sci. Eng. 134 (5) (2012) 051011.
[30] Z. Spitalsky, et al., Carbon nanotube-polymer composites: chemistry, processing, mechanical and electrical properties, Prog. Polym. Sci. 35 (3) (2010) 357–401.
[31] H. Canbolat, A novel level measurement technique using three capacitive sensors for liquids, IEEE Trans. Instrum. Meas. 58 (10) (2009) 3762–3768.
[32] S.C. Bera, et al., Study of a modified capacitance-type level transducer for any type of liquid, IEEE Trans. Instrum. Meas. 63 (3) (2014) 641–649.
[33] A.K. Au, et al., 3D-printed microfluidic automation, Lab Chip 15 (8) (2015) 1934–1941.
[34] K. Yu, Q. Ge, H.J. Qi, Reduced time as a unified parameter determining fixity and free recovery of shape memory polymers, Nat. Commun. 5 (2014).
[35] N. Hu, et al., Investigation on sensitivity of a polymer/carbon nanotube composite strain sensor, Carbon 48 (3) (2010) 680–687.
[36] A. Sanli, et al., Piezoresistive characterization of multi-walled carbon nanotube-epoxy based flexible strain sensitive films by impedance spectroscopy, Compos. Sci. Technol. 122 (2016) 18–26.
[37] L. Lin, et al., Towards tunable sensitivity of electrical property to strain for conductive polymer composites based on thermoplastic elastomer, ACS Appl. Mater. Interfaces 5 (12) (2013) 5815–5824.
[38] J.E.R. Bautista-Quijano, et al., Strain sensing, electrical and mechanical properties of polycarbonate/multiwall carbon nanotube monofilament fibers fabricated by melt spinning, Polymer 82 (2016) 181–189.
[39] H. Mei, et al., A flexible pressure-sensitive array based on soft substrate, Sens. Actuators A: Phys. 222 (2015) 80–86.
[40] O. Kanoun, et al., Flexible carbon nanotube films for high performance strain sensors, Sensors 14 (6) (2014) 10042–10071.
[41] J.A. Rogers, T. Someya, Y. Huang, Materials and mechanics for stretchable electronics, Science 327 (5973) (2010) 1603–1607.
[42] S. Yang, E. Ng, N. Lu, Indium tin oxide (ito) serpentine ribbons on soft substrates stretched beyond 100%, Extreme Mech. Lett. 2 (2015) 37–45.
[43] C.-C. Kim, et al., Highly stretchable: transparent ionic touch panel, Science 353 (6300) (2016) 682–687.
[44] A.J. Bandodkar, et al., Highly stretchable fully-printed CNT-based electrochemical sensors and biofuel cells: combining intrinsic and design-induced stretchability, Nano Lett. 16 (1) (2015) 721–727.
[45] Y. Zhang, et al., Polymer-embedded carbon nanotube ribbons for stretchable conductors, Adv. Mater. 22 (28) (2010) 3027–3031.
[46] Y. Zhu, F. Xu, Buckling of aligned carbon nanotubes as stretchable conductors: a new manufacturing strategy, Adv. Mater. 24 (8) (2012) 1073–1077.